01 Aug 1990

Double Excitation of He by Fast Ions

J. P. Giese

Michael Schulz
Missouri University of Science and Technology, schulz@mst.edu

J. K. Swenson

Harald Schone

et. al. For a complete list of authors, see https://scholarsmine.mst.edu/phys_facwork/1295

Recommended Citation

J. P. Giese and M. Schulz and J. K. Swenson and H. Schone and M. Benhenni and S. L. Varghese and C. R. Vane and P. F. Dittner and S. M. Shafroth and S. Datz, "Double Excitation of He by Fast Ions," *Physical Review A*, vol. 42, no. 3, pp. 1231-1244, American Physical Society (APS), Aug 1990.
The definitive version is available at https://doi.org/10.1103/PhysRevA.42.1231

Double excitation of He by fast ions

J. P. Giese,* M. Schulz,* J. K. Swenson,† H. Schöne, M. Benhenni,‡ S. L. Varghese,§
C. R. Vane, P. F. Dittner, S. M. Shafroth,‡ and S. Datz
Oak Ridge National Laboratory, P.O. Box 2008, Oak Ridge, Tennessee 37831-6377
(Received 16 January 1990)

Autoionization of He atoms following double excitation by electrons, protons, C^{Q+} ($Q=4-6$), and F^{Q+} ($Q=7-9$) ions has been studied. The electron-emission yields from the doubly excited $2s^2(^1S)$, $2s2p(^1P)$, and $2p^2(^1P)$ states were measured at the reduced projectile energy of 1.5 MeV/nucleon for observation angles between 10° and 60°. The results indicate excitation to the $2s^2(^1S)$ and $2p^2(^1D)$ states increases as approximately Q^3, while excitation to the $2s2p(^1P)$ state varies as approximately Q^2, where Q is the charge of the projectile. These charge dependences are significantly less than the Q^4 dependence expected in the independent-electron model, suggesting the interaction between the two target electrons is important in creating the doubly excited states.

I. INTRODUCTION

One of the fundamental problems in physics is how to understand properties of many-particle systems given our knowledge of one- and two-particle systems. Within the field of atomic collision physics, one approach to this problem has been to study the effects of electron-electron interactions in many-electron phenomena. The simplest model of many-electron processes is the independent-electron model (IEM). The IEM assumes each electron moves independently of the other electrons in the average potential of all the electrons and the nucleus. A great deal of experimental and theoretical effort has been directed toward studying deviations from the IEM predictions.[1,2] Such deviations are frequently attributed to electron-electron correlation, indicating the motions of the individual electrons are directly related. Attention has been particularly directed at the study of two-electron processes in two-electron systems. One of the simplest two-electron systems is created in the collision of bare projectiles with He atoms. Recent studies of double ionization[3,4] and transfer ionization[5,6] by fast, bare projectiles have clearly demonstrated in the importance of electron-electron interactions. This paper reports a study of double excitation of He by fast projectile ions.

The possible two-electron phenomena in the collision of bare projectiles with He include double excitation, excitation ionization, double ionization, transfer excitation, transfer ionization, and double transfer. Perturbative models of these phenomena are generally valid at projectile velocities much greater than the target electron velocities. The IEM mechanism involves the independent interaction of the projectile with each of the two target electrons. This second-order process has two strong projectile-electron interactions and does not involve any correlation of the electrons. The cross sections from this mechanism would be expected to vary as Q^4, where Q is the charge of the projectile. There are also first-order perturbative mechanisms which can produce two-electron phenomena. These first-order mechanisms can be conceptually divided into two groups, involving static and dynamic correlation of the target electrons. The dynamic mechanism involves the projectile interacting strongly with only one electron, with this electron then colliding with the other electron. This mechanism is a two-step process, but with only one projectile electron interaction. The static mechanism also involves a single interaction between the projectile and a target electron. The other electron undergoes a transition due to a final-state rearrangement of the target. This rearrangement can be attributed to the initial static correlation of the electrons, and is referred to as a "shake" process. The cross section due to either of these first-order mechanisms would be expected to vary as Q^2. Finally, quantum interference of the first- and second-order mechanisms could lead to a term in the cross sections proportional to Q^3.

One technique used to determine the importance of correlation in two-electron phenomena has been to examine the emission of the collision products as a function of their energy and scattering angle. Evidence of the dynamic correlation of the He electrons has been observed in ionization of one He electron accompanied by capture of the other He electron by the projectile (transfer ionization). When this process occurs via the first-order process, there is a critical scattering angle for the projectile at 0.55 mrad.[7] Measurements of the ratio of double to single ionization of He by 0.3–0.7 MeV protons have detected a peak at approximately 0.55 mrad.[7] Calculations have suggested a similar feature should appear as a peak in the angular distribution of the ionized electrons[8] or as a ridge in the energy and angular distribution of these electrons.[9] A recent measurement of the angular distribution of electrons emitted in the transfer ionization of He by 1-MeV protons has confirmed this prediction.[6]

Another technique used to observe correlation is to study the charge-state dependence of a particular process. It is possible to gain at least a qualitative estimate of the importance of correlation by observing deviations from the IEM prediction of Q^4 dependence. Double ionization

of He has been studied using electrons, anitprotons, protons, and more highly charged positive ions. Electrons[10] and antiprotons[3,4] were almost twice as effective as protons in doubly ionizing He in a broad range of velocities around 10 a.u. The dependence of the cross section on the sign of the charge was attributed to interference of the first- and second-order mechanisms. These results have also been interpreted as a charge-state-dependent correlation adjustment of the electron motion during the collision.[11–13] This adjustment for antiprotons and electrons increases the probability of ionizing one of the electrons on the condition that the other electron is also being ionized. This is effectively a second-order process where the two projectile-electron collisions *are* correlated. It is not yet clear which explanation is preferable, but both require correlated motion of the two electrons.

The object of the present work is to measure the dependence of double excitation of He on the charge, Q, of fast ($v \gg v_0$) projectile ions. Double excitation is conceptually somewhat simpler than the various two-electron ionization phenomena, where understanding of two correlated continuum electrons is needed. The doubly excited states of He all lie above the first ionization limit and decay almost exclusively via autoionization. This decay produces a He ion in the ground state and a free electron with an energy characteristic of the excited state. The double-excitation process may thus be identified experimentally by observing a structure at the characteristic energy in the energy spectra of the ionized He electrons. The doubly excited He states are well understood, and calculations are therefore more tractable than for ionization.[14] Finally, these states have definite quantum numbers, and comparison of the Q dependences for the different states may thus give more information on the relative importance of the proposed double-excitation mechanisms.

Double excitation of He has been extensively studied over the past few decades. The autoionizing states have been detected in inelastic scattering of electrons,[15–17] in photoabsorption,[18] and in energy spectra of autoionized electrons emitted following collisions with electrons,[19,20] ions,[21–24] and atoms.[25] Much of the existing research has been for electrons and singly charged ions at velocities less than a few a.u. Many of the common features of this earlier work, however, are relevant to the present study. The autoionized electrons can interfere with directly ionized electrons of the same energy.[26] As a result, the energy profiles and angular distributions of the emission lines due to autoionizing states can be asymmetric.[27] The asymmetry of the lines is most important at small electron emission angles and at higher projectile velocities. The Coulomb interaction between the autoionized electron and the receding projectile ion [post-collision interaction (PCI)] has been found to further distort the line profiles.[22,28] Double excitation at low velocities can be understood as due to electron promotion in the quasimolecule formed during the collision.[22] Atomic mechanisms, such as the perturbative models discussed above, become more important as the velocity is increased.

There has been only a limited amount of research on double excitation of He at higher velocities, especially using more highly charged projectiles. Double excitation due to electron impact has been observed at velocities above 7 a.u., but few quantitative results are available.[17,29] Similarly, the doubly excited states have been observed following impact by fast protons ($v=12.65$ a.u.) and O^{5+} ions ($v=8.66$ a.u.).[30] The only quantitative results using heavy ions are from the work of Arcuni and Schneider[24] using protons, He^{Q+} ($Q=1,2$), and Li^{Q+} ($Q=1$–3) ions for $v<4.47$ a.u. and from the work of Pedersen and Hvelplund[29] using protons and C^{Q+} ($Q=4$–6) ions at $v=8.57$ a.u. Arcuni and Schneider were primarily concerned with PCI effects, and found that PCI-induced observable distortions of the line profiles even at the high velocity limit of their data. They also determined that the total emission cross section of the three lowest-lying doubly excited states increased much more slowly with the projectile charge than the IEM prediction of Q^4. The work of Pedersen and Hvelplund, which included equal velocity electron projectiles, concentrated specifically on measuring the charge-state dependence of the double-excitation cross section. They found little significant difference between the emission yields due to protons and electrons, but their yields increased as approximately Q^4 for the C projectiles. Recent calculations by Fritsch and Lin[31] examined the double excitation of He by bare projectiles with charges up to 9 at velocities of 7.75 and 15.49 a.u. These calculations indicate the first-order mechanisms are important and sometimes dominate at these velocities. Our results extend the results of the two experimental groups to higher projectile charges and/or energies. The differential electron emission cross sections from the three lowest-lying doubly excited states of He have been measured following impact by electrons, protons, C^{Q+} ($q=4$–6), and F^{Q+} ($Q=7$–9) ion at $v=5.48$ a.u. and emission angles between 10° and 60°.

II. EXPERIMENT

The experiment was performed at the EN Tandem Facility of the Oak Ridge National Laboratory. Ion beams of 1.5-MeV p^+, 18-MeV C^{3+}, and 28.5-MeV F^{5+} were produced by the EN Tandem Van de Graaff accelerator. After charge and mass analysis, the carbon and fluorine ions were passed through a thin foil to obtain the desired charge states: C^{Q+} ($Q=4,5,6$) and F^{Q+} ($Q=7,8,9$). The ions were then analyzed again to select the final charge state and to direct the beam to the experiment. The electron beams of ~823 eV were produced with an electron gun which could be inserted in the experimental chamber immediately before the He gas cell. After passing through the gas cell, the beams were collected in a Faraday cup for normalization.

The gas cell and the essential components of the electron detector are shown in Fig. 1. The differentially pumped gas cell consisted of concentric cylinders with the inner cylinder defining the target region. Electrons produced in the gas cell passed through slits in both the inner and outer cylinders located at every 10° relative to the beam direction from 10° to 60°. It was not possible to

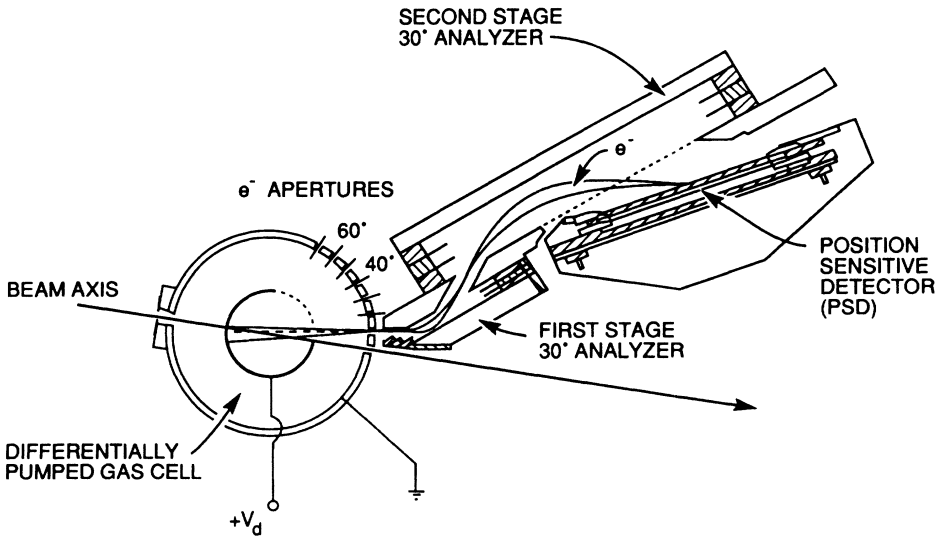

FIG. 1. The high-resolution electron spectrometer and differentially pumped gas cell.

reach angles greater than 60° with this spectrometer. The electrons exiting the gas cell were then energy analyzed in a two-stage 30° parallel-plate electron spectrometer and detected by a position-sensitive microchannel-plate array (MCP). The details of the spectrometer and MCP have been described elsewhere.[32] The autoionized He electrons have energies between 30 and 45 eV. These relatively low-energy electrons can be easily deflected by stray electromagnetic fields. Therefore, the entire apparatus was made from nonmagnetic materials and the gas cell and spectrometer are surrounded by a shield of high permeability magnetic material (μ metal). This reduces the residual magnetic field to less than 10 mG, which should not significantly deflect the 30–40 eV electrons studied here. Electric fields from surface charging were minimized by coating all metal surfaces exposed to the electrons with a conductive graphite coating. Finally, the projectile beams were collimated to 0.64×0.64 mm^2 with slits attached to the outer gas cell cylinder in order to prevent projectile ions from striking the inner cylinder. The He gas pressure within the inner cylinder was measured with a capacitance manometer and was typically set between 5 and 10 mTorr. This range of pressures was determined to be within the region of single-collision conditions by measuring the pressure dependencies of electron emission due to both direct and single ionization and to the double excitation resonances.

Electrons of energy E emitted in the gas cell were decelerated by applying a positive potential V_d to the inner cylinder while keeping the outer cylinder grounded. The spectra presented here were taken with $V_d=+10$ V and have an overall energy resolution of about 0.3 eV. The emission energy of an analyzed electron is given by

$$E=eV_p(ax+b)+eV_d\ , \tag{1}$$

where V_p is the analyzing voltage of the spectrometer, x is the position where the electron strikes the MCP, and a and b are constants. The spectra were required as a function of x with V_p fixed. Neither the microchannel plates nor the charge-collecting resistive anode have uniform counting efficiency as a function of position. Therefore, it is necessary to correct the measured spectra for their relative efficiency. This was done by scanning electrons of constant energy across the detector by varying the analyzing voltage. The transmission of the spectrometer as a function of the analyzing voltage is known,[32] so this scan can be converted to give the relative efficiency of the detector. The correction for relative efficiency was checked by noting that the electron emission yields for the $2p^2(^1D)$ state were constant as a function of position on the detector.

Absolute cross sections for electron emission were obtained by normalizing the present spectra to previous measurements of Ne K-shell Auger electron emission due to 1.5-MeV protons.[33] These Ne Auger electrons have energies between about 730 and 820 eV, much higher than the autoionized He electrons. It is certainly possible that there is a significant difference in efficiency for 800-eV Ne K-Auger electrons compared to 35-eV He electrons. In order to investigate this effect, the present emission cross sections were measured as a function of the impact energy of the electrons on the channel plates by varying the deceleration voltage. These cross sections were constant within the energy range of 15–45 eV. Below 15 eV, the measured cross section begins to decrease, presumably due to either losses from stray fields or from a decrease in the detection efficiency. Thus, within the energy range observed in the present data, the absolute efficiency of the MCP's was relatively constant. Previous studies of MCP efficiencies indicate that the absolute efficiency of an individual MCP can be relatively insensitive to the electron energy.[34] Furthermore, the present doubly differential electron-emission cross sections are consistent with previous measurements of p^++He at 1.5 MeV (Ref. 35) and of C^{6+}+He at 30° and 30 eV.[36,37] Therefore, while we have no direct empirical

measurement of the efficiency, we are reasonably confident that the absolute scale of the present data is correct.

III. RESULTS

The doubly differential electron-emission cross sections from He atoms at emission angles of 10, 20, and 40 deg relative to the beam axis are shown in Fig. 2 for collisions with 18-MeV C^{6+} projectiles. Similar spectra for 1.5-MeV proton projectiles are shown in Fig. 3. The energy of the autoionized electrons from the lowest-lying He states are indicated in Figs. 2(a) and 3(a). The dominant excitations in all our spectra were to the $2p^2(^1D)$ and $2s2p(^1P)$ states. The energy resolution of the spectrometer, about 0.3 V, was not sufficient to resolve the $2p^2$ and $2s2p$ states which are separated by only 0.24 eV. There were indications of population of the $2s^2(^1S)$ state in some of the spectra. Above 38 eV, several states were populated, with the strongest probably being the $2p3p(^1P)$. However, these lines were difficult to positively identify because of their small separations. None of the low-lying triplet states were populated, even with electrons and non-bare ions as projectiles. We saw no evidence in our data that the projectile electrons on the non-bare ions were active in these collisions. These projectile electrons are tightly bound, and, for the purposes of discussion and comparison, we treat the non-bare projectiles used here as point charges.

The continuum "background" in the spectra is from directly ionized electrons. The peak due to the $2p^2(^1D)$ and $2s2p(^1P)$ states in the carbon spectra clearly has the asymmetric "Fano" profile indicative of interference between directly ionized electrons and autoionized electrons. The asymmetry is strongest at small emission angles, in agreement with previous measurements.[27] Fano profiles are also present in the proton data, although the $2p^2+2s2p$ peak is much more symmetric for protons. This peak seems to become more symmetric at smaller angles for protons, opposite to the trend for carbon. Furthermore, the asymmetry of this peak is different for the proton data, which has a small dip on the high-energy side, than for the carbon data, which has a stronger dip on the low-energy side. These differences suggest that relative importance of the excitation to the $2p^2$ and $2s2p$ states might be different than that for carbon ions. How-

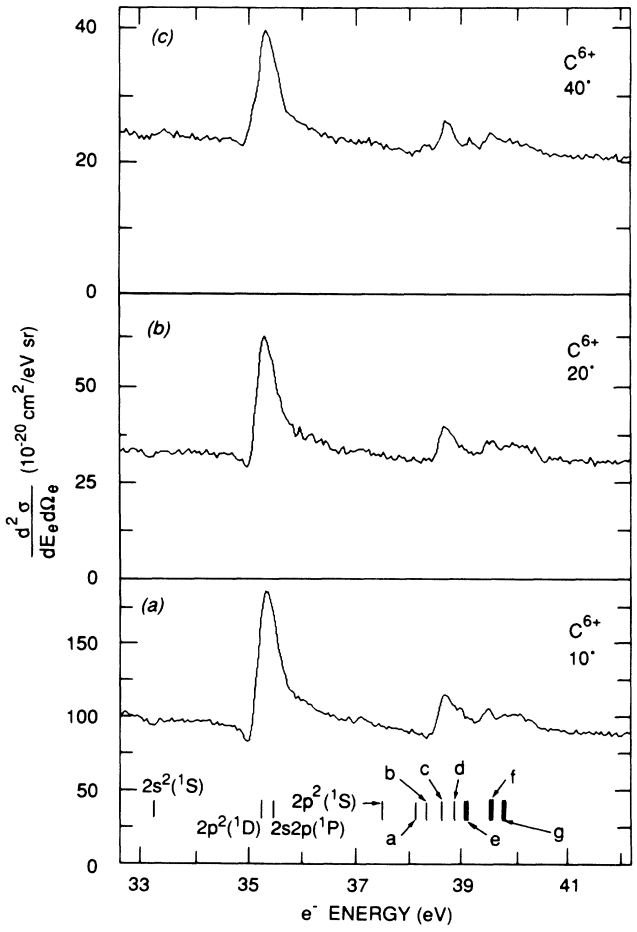

FIG. 2. Doubly differential electron-emission cross sections from He at (a) 10, (b) 20, and (c) 40 deg relative to the beam axis following collisions with 18-MeV C^{6+} projectiles. The positions of the lower-lying doubly excited He states are shown in (a). The higher-lying states are identified by letter and are: (a), $2s3p-(^1P)$; (b) $2s3s(^1S)$; (c), $2p3p(^1P)$; (d), $2p3p(^1D)$; (e), $2s3p+(^1P)$ and $2p3d(^1D)$; (f), $2s4p-(^1P)$, $2p3p(^1S)$, $2p3d(^1P)$, and $2s4s(^1S)$; (g), $2p4p(^1D)$ and $2s4p+(^1P)$.

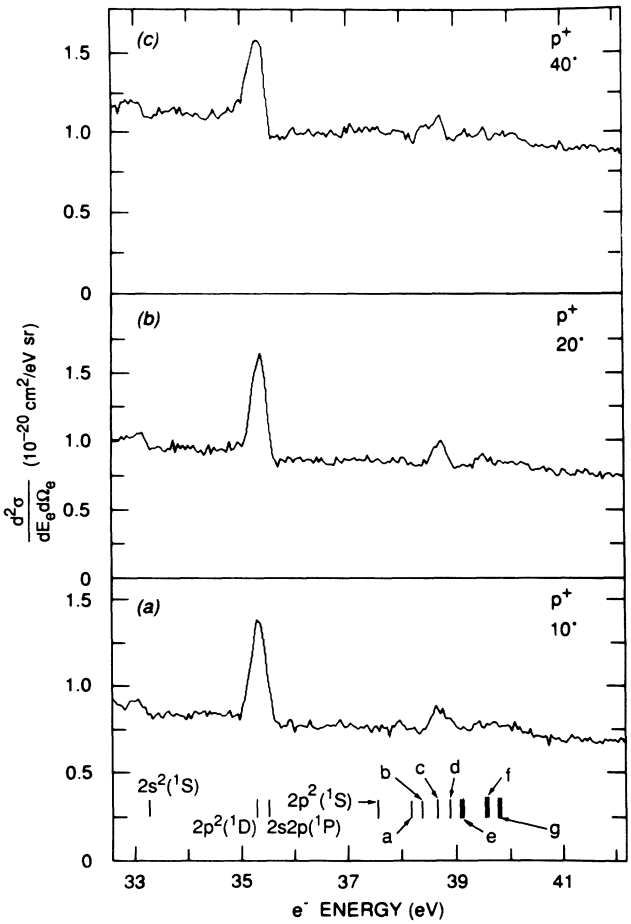

FIG. 3. Same as in Fig. 2 for 1.5-MeV proton projectiles.

ever, a quantitative analysis of the emission line profiles is necessary for more definite conclusions.

A. Autoionization theory

The experimental observation of an autoionized electron measures a physical state which can be defined by the electron energy and emission angle, $|E_e,\theta\rangle$. Following the development of Fano,[26] this physical state is most commonly described as a mixture of a discrete doubly excited state $|R\rangle$ and a continuum of single ionization states $|E_e^0,\theta\rangle$. The states $|R\rangle$ and $|E_e^0,\theta\rangle$ constitute a basis set which is chosen for convenience of calculation and for ease of understanding. The physical state can be formally represented as

$$|E_e,\theta\rangle = |R\rangle\langle R|E_e,\theta\rangle + \int dE_e^0 |E_e^0,\theta\rangle\langle E_e^0,\theta_e|E_e,\theta_e\rangle \ , \tag{2}$$

where the parameters $\langle R|E_e\theta\rangle$ and $\langle E_e^0,\theta|E_e,\theta\rangle$ are the expansion coefficients of the physical state on this basis set. We require that this basis set be complete and orthogonal and that the transformation from the physical state to this basis set be unitary.

The measured electron emission yield can be expressed as

$$\frac{d^2\sigma}{dE_e d\Omega_e} = |\langle E_e,\theta|T|i\rangle|^2 \ , \tag{3}$$

where $|i\rangle$ is the initial ground state of the He and T represents the perturbation caused by the projectile. The yield in terms of the common basis set is

$$\frac{d^2\sigma}{dE_e d\Omega_e} = |\langle E_e,\theta|R\rangle\langle R|T|i\rangle + \int dE_e^0 \langle E_e,\theta|E_e^0\rangle\langle E_e^0,\theta|T|i\rangle|^2 \ . \tag{4}$$

Clearly, the two terms on the right-hand side of this equation can interfere. The strength of the interference depends on the relative magnitudes of these two terms and on the relative phase between them. There is no *a priori* reason for the interference to be positive or negative. More simply, the interferences can be constructive or destructive. It is this interference between the amplitude for double excitation $\langle R|T|i\rangle$ and the amplitude for single ionization $\langle E_e^0,\theta|T|i\rangle$ that makes extraction of double-excitation cross sections from the data difficult.

A common parametrization of the doubly differential cross section for emission of electrons in the region of an isolated autoionizing resonance is called the Shore parametrization,[38]

$$\frac{d^2\sigma}{dE_e d\Omega_e} = f(E_e,\theta) + \frac{a(\theta)\varepsilon + b(\theta)}{\varepsilon^2+1} \ , \tag{5}$$

where

$$\varepsilon = \frac{2(E_e - E_r)}{\Gamma_r} \ , \tag{6}$$

E_r is the energy of the resonance, and Γ_r is the natural width of the resonance. The incoherent contribution to the differential cross section from direct ionization is given by $f(E_e,\theta)$, the asymmetry of the profile is described by $a(\theta)$, and the contribution of the discrete state to the cross section is given by $b(\theta)$. The latter can be illustrated by integrating over the electron energy to obtain the singly differential cross section,

$$\frac{d\sigma}{d\Omega_e} = F(\theta) + \tfrac{1}{2}\pi\Gamma_r b(\theta) \ , \tag{7}$$

where $F(\theta)$ now represents the incoherent contribution from direction ionization.

The differential emission yield, $d\sigma/d\Omega_e$, is approximately equal to the differential single-ionization yield for energies far away from the resonance energy, that is, for $\varepsilon \gg 1$, it is true that

$$\frac{d^2\sigma}{dE_e d\Omega_e} \simeq f(E_e,\theta) \equiv \frac{d^2\sigma_{\rm SI}}{dE_e d\Omega_e} \ . \tag{8}$$

Further, it can be reasonably assumed that the single-ionization yield would, in the absence of a resonance, vary smoothly with energy. The data is therefore fit by first determining $f(E_e,\theta)$ far from the resonance and extrapolating through the region of the resonance. The parameters $a(\theta)$ and $b(\theta)$ are then determined from the shape of the spectra in the region of the resonance. $a(\theta)$ and $b(\theta)$ can in principle be positive or negative. The typical Fano profile has a dip in the ionization background followed by a peak with a high-energy tail, or vice versa. However, depending on the relative magnitudes of $a(\theta)$ and $b(\theta)$, the resonance can have any shape ranging from a pure dip (or window) in the background to a pure Lorentzian peak on top of the background.

The relationship between $b(\theta)$ and the double-excitation cross section can be found by integrating Eq. (7) over the electron emission angle to obtain the total emission cross section,

$$\sigma = \sigma_{\rm SI} + \frac{\pi\Gamma_r}{2}\int b(\theta)d\Omega_e = \sigma_{\rm SI} + \frac{\pi\Gamma_r}{2}B \ . \tag{9}$$

The total cross section in terms of the preferred basis set is

$$\sigma = \int\int d\Omega_e dE_e |\langle E_e,\theta|T|i\rangle|^2 = \int\int d\Omega_e dE_e |\langle E_e,\theta|R\rangle\langle R|T|i\rangle + \int dE_e^0 \langle E_e,\theta|E_e^0,\theta\rangle\langle E_e^0,\theta_e|T|i\rangle|^2 \ . \tag{10}$$

Using the orthonormality and completeness of the basis set, this expression can be simplified to

$$\int\int d\Omega_e dE_e |\langle E_e,\theta|T|i\rangle|^2 = \int\int d\Omega_e dE_e |\langle E_e^0,\theta|T|i\rangle|^2 + |\langle R|T|i\rangle|^2 . \quad (11)$$

The last term in this equation $|\langle R|T|i\rangle|^2$ is the double-excitation cross section. Examining Eq. (7), it is possible to see that $b(\theta)$ is proportional to the single differential emission yield minus the extrapolated single-ionization background. Rearranging Eq. (11) gives

$$\int d\Omega_e \left[\int dE_e (|\langle E_e,\theta|T|i\rangle|^2 - |\langle E_e^0,\theta|T|i\rangle|^2)\right] = |\langle R|T|i\rangle|^2 \equiv \sigma_{\rm DE} , \quad (12)$$

where the term in large parentheses is proportional to $b(\theta)$. Equation (12) is important because it gives the relationship between the measured electron emission yield and the calculable single-ionization and double-excitation cross sections. Further, Eq. (12) shows that $B = \int b(\theta) d\theta_e$ is directly proportional to the double-excitation cross section. Note that while $b(\theta)$ can be positive or negative, the integral of $b(\theta)$ over the electron energy and emission angle represents a cross section and *must be positive*. If $b(\theta)$ is negative at some angles, it must therefore become positive at other angles in order for B to be positive.

The striking asymmetric line shapes of our spectra are an indication that the interference between double excitation and single ionization strongly affects the observed electrons. The above analysis shows that it is, in principle, possible to remove these interference effects and obtain the double-excitation cross section by integrating the difference between the measured electron emission yield and the extrapolated single-ionization yield over both the electron energy and the electron emission angle. However, due to the small separation of the $2p^2(^1D)$ and $2s2p(^1P)$ states, it is not possible to obtain individual cross sections for these two states by this process. Instead a more detailed analysis of the line shape for each state is necessary, using, for example, the Shore parametrization.

The peak profiles can also be represented by the Fano parametrization,[26] which is written as

$$\frac{d^2\sigma}{dE_e d\Omega_e} = f_{\rm back}(E_e,\theta) + f_{\rm res}(\theta)\frac{[\tilde{q}(\theta)+\varepsilon]^2}{\varepsilon^2+1} , \quad (13)$$

where $f_{\rm back}(E,\theta)$ represents transitions to states of the continuum which do not interact with the discrete state, $f_{\rm res}(\theta)$ represents transitions to states which do interact with the discrete state, and ε is defined as in Eq. (6). The dimensionless parameter $\tilde{q}$ is a measure of the asymmetry of the profile but is independent of the magnitude of the cross section. Note that $\tilde{q}$ is not the same as the Fano shape parameter q.[26] The latter was derived to describe the shape of the resonance in the *projectile* scattering angle and final energy. The relationship of $\tilde{q}$ to the shore parameters is given by the relationship

$$\tilde{q}(\theta) = \frac{b(\theta) + \{[b(\theta)]^2 + [a(\theta)]^2\}^{1/2}}{a(\theta)} . \quad (14)$$

When the absolute value of $\tilde{q}$ is very large, the peak is nearly Lorentzian. When $\tilde{q}$ is approximately zero, the peak becomes a symmetric dip or window in the continuum. The profile is asymmetric for intermediate values of $\tilde{q}$, with negative values corresponding to profiles with a dip on the high-energy side of the resonance, and positive values to a dip on the low-energy side.

The Shore parametrization and the Fano parametrization are equivalent.[2,24,39] We have chosen to analyze our data by fitting the measured spectra using the Shore parameters. This was done because $b(\theta)$ is proportional to the contribution of the double-excitation resonance to the differential-ionization cross section. Thus $b(\theta)$ can be used to compare the excitation by different projectiles. The integral of b over the electron emission angle is used here to estimate the dependence of the total yield on the projectile charge. The asymmetry parametr $\tilde{q}$ is used here only for qualitative comparison of the profiles due to different projectiles.

B. Data analysis

A least-squares fitting procedure was used to extract the Shore parameters from the measured spectra. The theoretical line shape was

$$\frac{d^2\sigma}{dE\, d\Omega} = C(E,\theta) + \frac{D(E,\theta)}{E^2} + \sum_j \frac{b_j(\theta) + a_j(\theta)\varepsilon_j}{\varepsilon_j^2+1} , \quad (15)$$

where $C(E,\theta)$ and $D(E,\theta)$ were parameters used to fit the background due to direct ionization. The other parameters were as defined in Eq. (5) with subscripts added to indicate the individual resonances. The sum is over the different resonances included in the fit. This line shape was folded with the spectrometer function to obtain a theoretical spectrum. The spectrometer function was a Gaussian with a full width at half maximum of 0.3 eV. This width is proportional to the width of the spectrometer entrance slit and to the spectrometer plate voltage. The Gaussian width used here was determined from spectra of electron beams taken directly from the electron gun with the spectrometer at 0°.

The theoretical spectra were fit to the measured spectra by adjusting the background parameters $C(E,\theta)$ and $D(E,\theta)$ and the Shore parameters $a_j(E,\theta)$ and $b_j(E,\theta)$. The measured spectra were fit only in the region of the four lowest-lying resonances of He, from 32.5 to 37.5 eV.

TABLE I. The autoionization energies and widths (Refs. 40 and 41) of the lowest-lying doubly excited states of He.

State	Energy (eV)	Width (eV)
$2s^2(^1S)$	33.28	0.138
$2p^2(^1D)$	35.29	0.0723
$2s2p(^1P)$	35.53	0.0411
$2p^2(^1S)$	37.55	0.0067

The autoionization energies and decay widths of these states, the $2s^2(^1S)$, $2p^2(^1D)$, $2s2p(^1P)$, and $2p^2(^1S)$ states, are shown in Table I, and the energies are indicated in Fig. 2(a). No significant, reproducible contribution of the $2p^2(^1S)$ state was seen in our spectra, and hence this state was not included in the fit. The energy separations of these resonances and their widths are known and were fixed in the fitting procedure. Due to surface charging within the spectrometer, the absolute-energy calibration varied by a few percent among different sets of data. Thus, the location of the $2p^2(^1D)$ state was also used as a fitting parameter.

Several of the assumptions made in fitting the data with Eq. (15) can, in principle, significantly affect the accuracy of the interpretation and therefore merit explicit examination. First, the Shore parametrization strictly applies only to isolated resonances. As can be seen in Table I, the $2p^2(^1D)$ and $2s2p(^1P)$ states are separated by only a few resonance widths. These states can interfere, and this interference can affect their relative intensities by as much as $\pm 22\%$.[42] The present available experimental evidence, however, suggests this effect does not significantly alter the resonance profiles. Measurements of double excitation of He by protons with energies below 150 keV showed that this state-to-state interference has a much smaller effect on the profiles than the state-to-continuum interference.[28] Similar studies with more highly charged He and Li ions at energies up to 500 keV/nucleon also concluded that the state-to-state interference was very small and did not affect the analysis of the profiles.[43] Thus we have not attempted to account for the interference of these states in our fits.

The present analysis also assumes the interaction of the emitted autoionization electron with the receding projectile does not significantly affect the measured profiles. Such post-collision interactions (PCI) are generally assumed to be important only when the projectile velocity is comparable to or smaller than the emitted electron's velocity.[24,43,44] However, Arcuni and colleagues have shown that PCI does affect the profiles, even at 500 keV/nucleon, where the projectile velocity is already several times larger than the electron velocity.[24] The change in profile shape due to PCI was found to be small at this energy, and the conclusion was that PCI predominantly affected the profile symmetry but not its magnitude. Our present data is at 1500 keV/nucleon, where PCI effects should be even smaller. Given that our resolution is worse than that of Arcuni *et al.*, it is doubtful we could distinguish PCI effects. Furthermore, we are primarily interested in the magnitudes of the profiles. Therefore, we have not included PCI in our analysis.

IV. DISCUSSION

The fits of the spectra due to the four bare projectiles used here are shown in Fig. 4 for an electron emission angle of 10°. The total fit is a superposition of the profiles due to the individual resonances, and is shown as a dashed line. As mentioned above, the $2p^2(^1D)$ and $2s2p(^1P)$ states are not resolved in these spectra. However, these two states are relatively isolated from the other doubly excited states. As a result, the contribution of each to the total line shape *is* discernible. This point has been noted before and is especially true when the profiles are very asymmetric.[28] Asymmetric profiles can modify the continuum above and below the resonance energy over an energy range which is several times the width of the state. This can be seen in Fig. 4, where the fit due to the $2s^2(^1S)$ and $2p^2(^1D)$ states is shown as a dotted line, and the fit due to the $2s^2$ and $2s2p$ states is shown as a dashed-dotted line. The asymmetry of the $2p^2$ and $2s2p$ states clearly disturbs the continuum even as far away as the energy of the $2s^2$ resonance. Thus, though we could not clearly resolve the $2p^2$ and $2s2p$ states, it was possible to extract some information on their individual Shore parameters.

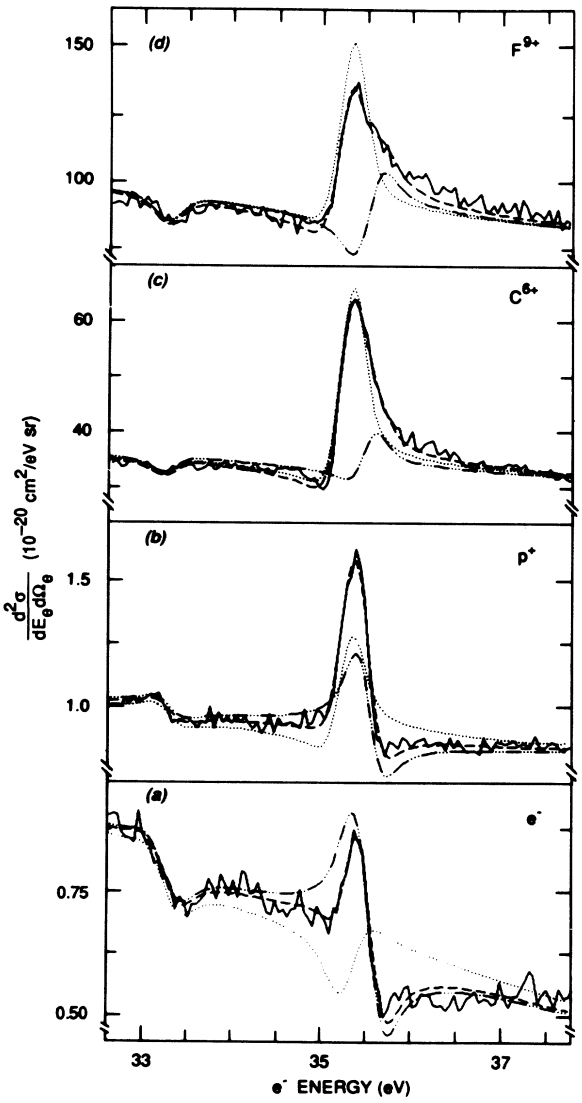

FIG. 4. The fits of Fano profiles to the doubly differential emission cross sections for (a) electron, (b) proton, (c) C^{6+}, and (d) F^{9+} projectiles at 10 deg. The dashed line is the total fit, the dotted line includes contributions of only the $2s^2$ and $2p^2$ resonances, and the dashed-dotted line includes only the $2s^2$ and $2s2p$ resonances.

TABLE II. The asymmetry parameters $\tilde{q}$ for the $2s^2(^1S)$, $2p^2(^1D)$, and $2s2p(^1P)$ states at 1.5 MeV/nucleon due to electrons, protons, C^{6+}, and F^{9+}.

Projectile angle (deg)	e^-	p^+	C^{6+}	F^{9+}
		$2s^2(^1S)$		
10		−0.840	0.270	−0.027
20	−0.947	−0.877	0.278	0.058
30	−0.945			
40	−0.910	−0.828	0.523	
50	−0.903			
60			0.655	
		$2p^2(^1D)$		
10		4.09	3.78	4.56
20	0.354	3.09	5.10	8.50
30	0.241			
40	0.113	2.59	8.76	
50	0.201			
60			6.05	
		$2s2p(^1P)$		
10		−1.71	1.80	0.858
20	−1.31	−1.55	2.61	0.762
30	−1.38			
40	−1.36	−1.85	2.35	
50	−1.20			
60			3.72	

There are three main sources of error in the present fitting procedure. The first two are the absolute normalization of the spectra and the correction of the spectra for the relative efficiency of the detector. As mentioned above in Sec. II, we believe these errors are small. Furthermore, these two errors should not affect comparison of spectra due to different projectiles. The dominant error for the $2p^2$ and $2s2p$ states comes from our inability to clearly resolve these states. We attempted to estimate the size of this systematic error by creating simulated spectra with known values of the Shore parameters. These simulated spectra were fit using the same procedure as for the measured spectra. We concluded that the relative error in $b_j(\theta)$ is about 25% for the $2p^2(^1D)$ state and 40% for the $2s2p(^1P)$ state. The difference in these errors is due to the larger width of the $2p^2$ state which spreads the effect of its asymmetry over a larger energy region. The $2p^2$ state is also more strongly populated in most of our spectra. The error in the $2s^2(^1S)$ state is about 35% and is due primarily to its low intensity.

The qualitative comparison of the line shapes due to protons and C^{6+} ions in Figs. 2 and 3 can now be supported quantitatively by calculating the Fano shape parameter $\tilde{q}$ from the Shore parameters using Eq. (14). The values of $\tilde{q}$ for each of the analyzed states are shown in Table II for the four bare ions as a function of θ. These $\tilde{q}$ change significantly for each state as the projectile charge is changed, and for some projectiles change significantly over the angular range studied here. The $\tilde{q}$ for the $2p^2(^1D)$ state are large and positive for the heavy ions (p^+, C^{6+}, F^{9+}) and this state appears as a nearly symmetric peak with a small low-energy dip in Figs. 4(b)–4(d). The $\tilde{q}$ for electrons are much smaller and the $2p^2$ state appears as almost purely a dip in Fig. 4(a). The $2s2p(^1P)$ state is generally more asymmetric than the $2p^2(^1D)$ and has correspondingly smaller $\tilde{q}$. The $2s2p$ state has positive $\tilde{q}$ for C and F ions, but negative values for electrons and protons. Thus, the asymmetry of the profile flips, with the dip on the low-energy side in Figs. 4(c) and 4(d) and on the high-energy side in Figs. 4(a) and 4(b). The $\tilde{q}$ for the $2s^2(^1S)$ state also change sign for C and F ions compared to electrons and protons. The $2s^2$ $\tilde{q}$ are relatively small and this state appears as a dip or shoulder in the continuum. The change in the profiles as the projectile charge increases may be an indication that the dominant excitation mechanism is also changing.

The differential yields due to each resonance are proportional to $\frac{1}{2}\pi\Gamma_j b(E,\theta)$ [see Eq. (7)]. These yields are given in Table III for bare projectiles at all the angles measured here. The most interesting feature of Table II is that the $2s^2$ yields due to all projectiles and the $2p^2$ yields due to electrons are negative for all the angles measured here. The interference between double excitation and single ionization is thus almost completely destructive in these cases. Notice also that the differential yields for all three states were relatively independent of θ over the angular region studied here, especially for the heavy ions. The angular dependence of the $2p^2$ yields is illustrated in Fig. 5. Note that for ease of comparison, the *absolute values* for the $2p^2$ yields due to electrons were plotted. The apparent independence of our results on θ may be due to the limited angular range of our data. This is certainly true for the cases where b is negative.

TABLE III. The electron emission yields in units of 10^{-21} cm^2/sr for the $2s^2(^1S)$, $2p^2(^1D)$, and $2s2p(^1P)$ states at 1.5 Mev/nucleon due to electrons, protons, C^{6+}, and F^{9+} ions.

Projectile angle (deg)	e^-	p^+	C^{6+}	F^{9+}
		$2s^2(^1S)$		
10		−0.0452	−9.16	−54.50
20	−0.0484	−0.0426	−10.10	−45.60
30	−0.0652			
40	−0.0680	−0.0640	−7.12	
50	−0.0784			
60			−8.40	
		$2p^2(^1D)$		
10		1.40	139	382
20	−0.96	1.60	127	344
30	−1.20			
40	−1.79	1.40	131	
50	−1.89			
60			143	
		$2s2p(^1P)$		
10		0.476	24.2	22.4
20	0.764	0.590	25.6	31.6
30	1.06			
40	1.12	0.388	29.0	
50	0.824			
60			20.4	

Following the discussion in Sec. III A, the integral of these yields over all emission angles is the double-excitation cross section and must be positive. Thus, we can predict with reasonable confidence that the $2s^2$ yields for all projectiles and the $2p^2$ yields for electrons must become positive at large emission angles.

Other measurements of these yields for fast projectiles as a function of emission angle have been made over the entire range of angles, and show stronger angular dependences than the present data. Arcuni and Schneider[24] observe a decrease in the yields with increasing θ using Li and He ions at 0.5 MeV/nucleon. Pederesen *et al.*[29] measured the sum of the $2p^2(^1D)$ and $2s2p(^1P)$ states at 1.84 MeV/nucleon and, except for electrons, observed a similar decrease in the yields with increasing θ. The measurements of Pedersen *et al.* are closest in projectile energy to our results and should give nearly the same result. Their results for electrons, protons, and C^{Q+} (Q=4–6) are shown with open symbols in Fig. 5. Their results for protons, C^{5+}, and C^{6+} are consistently higher than the present results, and show a stronger angular dependence, even over this limited range of angles. The apparent agreement of the two data sets for the yields due to electrons is deceptive. Recall that the present $2p^2$ yields due to electrons were negative. The sum of the present $2p^2$ and $2s2p$ yields is, in fact, negative at all our observation angles, while the yields of Pedersen *et al.* were always positive. Thus, the two data sets actually give very different results for electrons. Due to their poorer energy resolution, Pedersen *et al.* did not attempt to analyze the Fano profiles. Instead, their yields were obtained by subtracting the continuum background from the data. Their procedure is consistent with Eq. (12) and should give the correct double-excitation cross section for the sum of the $2p^2$ and $2s2p$ states. The two different procedures for obtaining the yields are both sensitive to the extrapolation of the background through the region of the resonance, especially at small emission angles. The difference in the methods may therefore be responsible for the differences between the two data sets.

Perhaps more interesting than the angular dependence is the dependence of the total emission yields on the projectile charge. Given the limited angular range of the present data and the fact that the differential yields were sometimes negative, it was not possible to accurately calculate double-excitation cross sections from the present data. We have attempted to estimate a total yield by assuming the electron emission is isotropic for all three states studied here. The total yields were then calculated as in Eq. (9) using the average measured value of $b_j(\theta)$. These yields are shown in Table IV for each state and projectile. This procedure is clearly flawed for the cases where $b_j(\theta)$ was negative, because it gives a negative cross section. Further, if in the other cases the differential yields to decrease at large emission angles as in the data of Pedersen and Hvelplund,[29] then our treatment of the data could overestimate the total yields by as much as 50%. Due to these limitations, the total "averaged" yields presented here can only be used to qualitatively compare the population of these states at small angles.

As discussed in the introduction, double-excitation

mechanisms which are first order in the projectile-electron interaction will produce cross section which vary as Q^2, while mechanisms which are second order will vary as Q^4. It is natural when using this model to parametrize[3,4] the total double-excitation cross section by

$$\sigma_t(Q)=\alpha Q^2+\beta Q^3+\gamma Q^4 , \tag{16}$$

where β is proportional to the strength of the interference term between first- and second-order mechanisms. It is not clear whether the perturbative model which leads to Eq. (11) is valid for the relatively high charge states of the C and F projectiles studied here. Measurements of the total single excitation[45] and total single ionization[46] of He at similar velocities to those studied here have shown that both of these processes begin to saturate at projectile charges between 6 and 10. These results certainly suggest that the double-excitation mechanisms could also be saturated. However, the present measurements of the differential electron emission yield include the "background" process of single ionization. As can be seen in Fig. 4, the "background" differential single-ionization cross section between 30 and 45 eV increases almost exactly as Q^2, as would be expected from the perturbative first Born model, and is not saturated. The differential yields from the doubly excited state are much smaller than the differential-ionization cross sections measured over the same electron energy range. Thus, it seems reasonable to assume that saturation effects do not strongly affect the yields measured here.

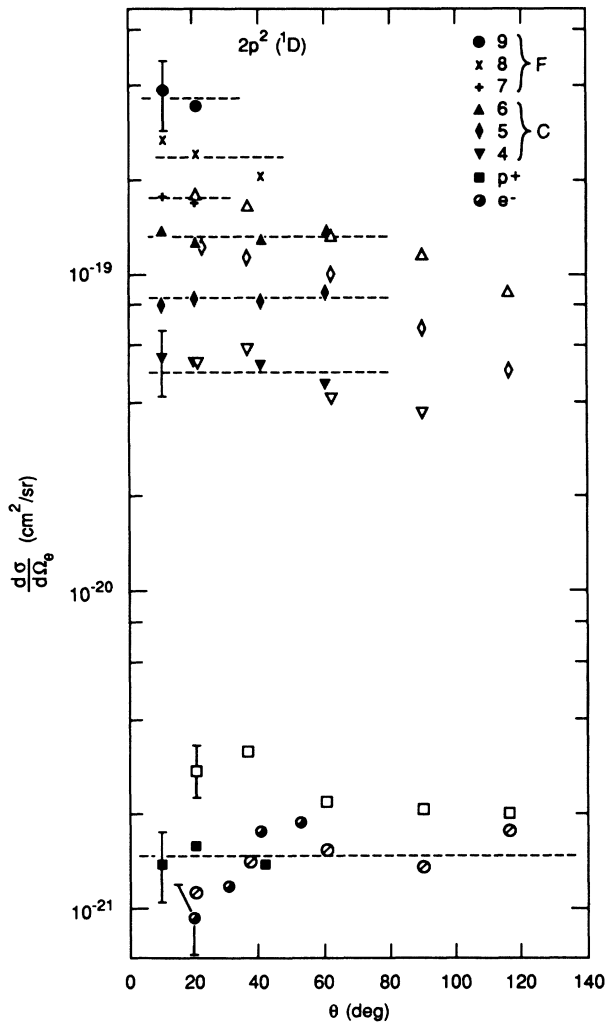

FIG. 5. The differential emission cross sections $(d\sigma/d\Omega)$ (cm^2/sr), from the $2p^2(^1D)$ state after excitation by electrons, protons, carbon ions, and fluorine ions at 1.5 MeV/nucleon. The open symbols represent the data of Pedersen and Hvelplund (Ref. 29). The dashed lines indicate the average cross section for each projectile. The yields due to electrons are negative at these angles, so the absolute value of the yields was plotted here for comparison of the angular dependence only (see text).

The data will be compared to the recent calculations of total double-excitation cross sections by Fritsch and Lin.[31] This comparison of our differential yields averaged over a limited angular range to their total cross sections can only be qualitative. Fritsch and Lin used a one-center atomic orbital expansion in a coupled channels calculation which included the electron-electron interactions between correlated He wave functions. The excitation cross sections to the $2s^2(^1S)$, $2p^2(^1D)$, $2s2p(^1P)$, and $2p^2(^1S)$ states were calculated for projectiles with charges -1, 1, 2, 4, 6, and 9 at 1.5 and 6 MeV/nucleon. Hypothetical projectiles with charges of -2 and -6 were included for comparison. The results for the projectile charges of interest here are included in Table IV.

Let us first examine the importance of the first- and second-order mechanisms by considering the relative magnitudes of excitation to the individual states by *protons*. As seen in Table III, the ^1D state has a slightly higher differential yield than the ^1P state, with the ^1S state more than an order of magnitude smaller and negative. This disagrees strongly with the cross sections of Fritsch and Lin, where the ^1P state is by far the largest, followed by the ^1S state and then the ^1D state. Fritsch and Lin also find that excitation of the $2p^2(^1S)$ state is comparable in magnitude to excitation of the $2p^2(^1D)$, while the data show no significant population of this state. The importance of these disagreements can be understood by considering the relative likelihood of excitation of the states via the first- and second-order mechanisms.

The largest excitation process will certainly be the dipole-allowed single excitation to the $1s2p(^1P)$ state. In the first-order mechanism, the $2s2p$ state can be populated via this excitation followed by a shake transition from $1s2p$ to $2s2p$. The excitation of the $2p^2(^1D)$ state via this intermediate state should be much smaller because the shake from $1s2p$ to $2p2p$ is not strictly an allowed transition. The $2s^2(^1S)$ state could be excited via a non-dipole-allowed excitation to the $1s2s$ intermediate state followed by a shake to $2s2s$. Thus, from the first-order mechanisms, we would expect the yields for the ^1P state to be the largest, followed most probably by the ^1S state and then the ^1D state. This is precisely the ordering of the results of Fritsch and Lin. The second-order mechanisms can be modeled as two successive single excitations. The excitation of the $2p^2(^1D)$ state would involve two dipole-allowed transitions, and should have the

TABLE IV. The experimental total averaged electron emission yields and theoretical double-excitation cross sections in units of 10^{-20} cm^2 for the $2s^2(^1S)$, $2p^2(^1D)$, and $2s2p(^1P)$ states at 1.5 MeV/nucleon due to electrons, protons, C^{9+}, and F^{9+} ions. The results for the ^1D and ^1P are summed in the last three columns in order to compare to the data of Pedersen and Hvelplund (Ref. 29).

	$2s^2(^1S)$		$2p^2(^1D)$		$2s2p(^1P)$		$2p^2(^1D)$ and $2s2p(^1P)$		
Projectile	Expt.	Theory[a]	Expt.	Theory[a]	Expt.	Theory[a]	Expt. 1	Expt. 2[b]	Theory[a]
e^-	0.0816	0.73		0.27	1.17	3.3	3.05	1.92	3.57
p	0.0318	0.74	1.84	0.48	0.608	3.0	2.45	2.75	3.48
C^{4+}	4.56	15.6	63.8	38.0	8.32	60.0	72.1	47.2	98.0
C^{5+}	8.08		104		20.6		124.6	100.4	
C^{6+}	10.9	51.6	170	156	31.1	162	201.1	149.9	318.0
F^{7+}	16.8		218		22.8		241		
F^{8+}	45.4		299		40.7		340		
F^{9+}	62.9	198	456	603	33.9	513	489		1116

[a]Fritsch and Lin (Ref. 31).
[b]Pedersen and Hvelplund (Ref. 29).

largest yields from the second-order mechanism. Excitation to the $2s2p$ and $2s^2$ states involves one and two nondipole-allowed transitions, respectively, and should be correspondingly smaller. The ordering from the second-order mechanisms would be ^1D, ^1P, and ^1S, which agrees with the present data. Thus, the theoretical results suggest the first-order mechanisms are dominant for excitation by protons, while the data suggest the second-order mechanisms are more important.

The overall charge dependence of the yields from individual states also provides information on the relative importance of these mechanisms. The dependence of the $2p^2(^1D)$ state is illustrated in Fig. 6, and clearly lies somewhere between Q^2 and Q^3. The dashed line in Fig. 6 is a least-squares fit of the data to Eq. (11), with $\alpha=(1.938\pm0.321)\times10^{-20}$ cm^2, $\beta=(0.277\pm0.235)\times10^{-20}$ cm^2, and $\gamma=(0.0158\pm0.0330)\times10^{-20}$ cm^2. The relatively large value of α indicates the first-order processes dominate excitation of the ^1D state even for the most highly charged ions. Due to the magnitude of the error in the present results, the use of this parametrization may be somewhat questionable. This can be shown by fitting the data with the simpler parametrization

$$\sigma_t(Q)=AQ^B\,, \tag{17}$$

which gives $A=(1.92\pm0.37)\times10^{-20}$ cm^2 and $B=2.47\pm0.43$. This fit is equally as good as the more complex parametrization shown in Fig. 6. Thus, we feel that trying to interpret the relative magnitudes of α, β, and γ may not be justified by the present data. No matter which parametrization is used, however, it is clear that the first-order process is dominant. This result is contrary to conclusions reached from the relative magnitudes of excitation to the three states by protons.

The theory and data for the ^1D state are certainly in reasonable qualitative agreement in charge dependence. Both theory and data suggest that the second-order mechanisms become more important for highly charged ions. However, the theoretical cross sections given in Table IV show a much stronger Q dependence for the ^1D state than in the data. This can be clearly seen by plot-

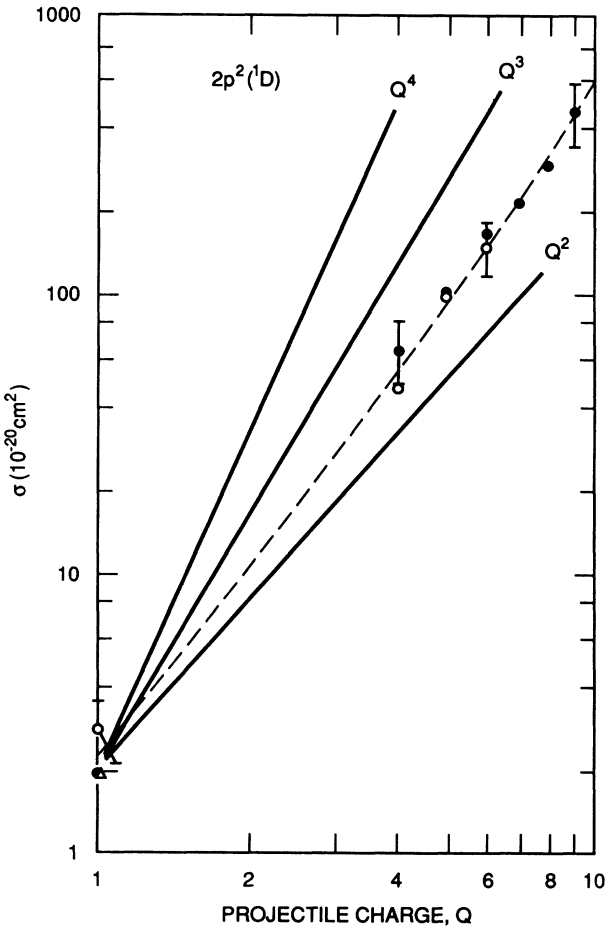

FIG. 6. The total averaged emission cross section from the $2p^2(^1D)$ state as a function of the projectile charge (see text). Electrons are indicated with triangular symbols. The open symbols represent the data of Pedersen and Hvelplund (Refs. 29 and 47). The dashed line is a fit of Eq. (16) to the data as described in the text. The solid lines indicate the slopes of Q^2, Q^3, and Q^4 dependence.

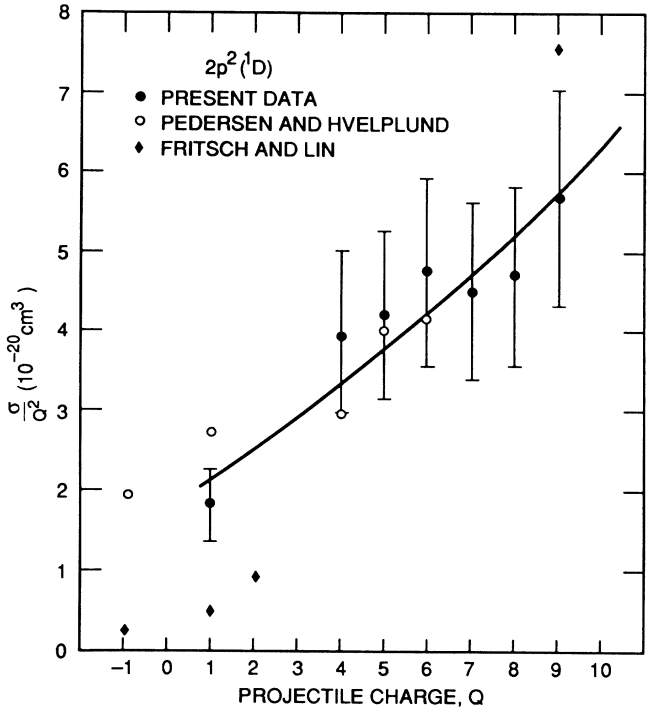

FIG. 7. The total averaged emission cross section for the $2p^2(^1D)$ state divided by the square of the charge of the projectile. The open circles represent the data of Pedersen and Hvelplund (Refs. 29 and 47), while the diamonds represent the calculations of Fritsch and Lin (Ref. 31). The solid curve is the fit to Eq. (11) and is not meant to imply that the cross section for a neutral projectile is not zero.

ting the total emission yield divided the projectile charge squared, σ/Q^2, as is done in Fig. 7. The theoretical values are much smaller than the data for electrons and protons, but increase much more rapidly for the highly charged ions at a rate slightly greater than Q^3. The theoretical results thus suggest that while the first-order mechanisms are dominant for low charged projectiles, the second-order mechanisms become important for highly charged projectiles. This explanation agrees with the experimental results found from the fit of Eq. (16) where the coefficient α was much larger than γ. The fit of Eq. (16) to the data is shown again in Fig. 7 as a solid curve. Although there is a large uncertainty in this fit, it does qualitatively agree with the theoretical result.

This conclusion is supported by the results of Arcuni and Schneider,[24] who also fit their data for the ^1D state using the simpler parametrization [Eq. (17)]. They found $B=2.58$ for excitation to the ^1D state by protons, Li, and He projectiles at 500 keV/nucleon. The results of Pedersen and Hvelplund at 1.84 MeV/nucleon (Ref. 29) are also in agreement with the present results in both magnitude and charge dependence. Their total yields for the sum of the ^1D and ^1P states are shown with open symbols in Figs. 6 and 7, and are compared to the present results for the sum of these two states in Table IV. Their yields for protons are slightly higher than our results, while their yields for C ions are somewhat lower than our results and show a much stronger Q dependence of nearly Q^4. However, as is emphasized in Fig. 7, the two data sets have almost the same qualitative Q dependence over the entire range of projectile charges, with the present results having a slightly stronger overall dependence. These results indicate that the higher-order mechanisms (Q^3 and Q^4) are important for highly charged projectiles where the IEM mechanism should be relatively more important. However, it is not possible from the currently available data to distinguish between Q^3 and Q^4 contributions.

It is important to emphasize at this point the significance of the similarity of the yields due to protons and electrons for the $2s^2$ and $2s2p$ states. Although the use of Eq. (16) may be problematic for highly charged ions, it should be valid for electrons and protons. We would therefore expect a significant difference between the yields due to electrons and protons if the interference term proportional to Q^3 were important. As can be seen in Fig. 6 for the ^1D state, the yields of Pedersen and Hvelplund due to electrons and protons were quite similar with protons giving slightly larger yields. Furthermore, as can be seen in Fig. 8 and in Table III, the differential yields for the ^1S and ^1P states due to electrons and protons have the same sign and are quite similar given the magnitude of the relative errors, with the electrons producing slightly higher yields. The data thus indicate that

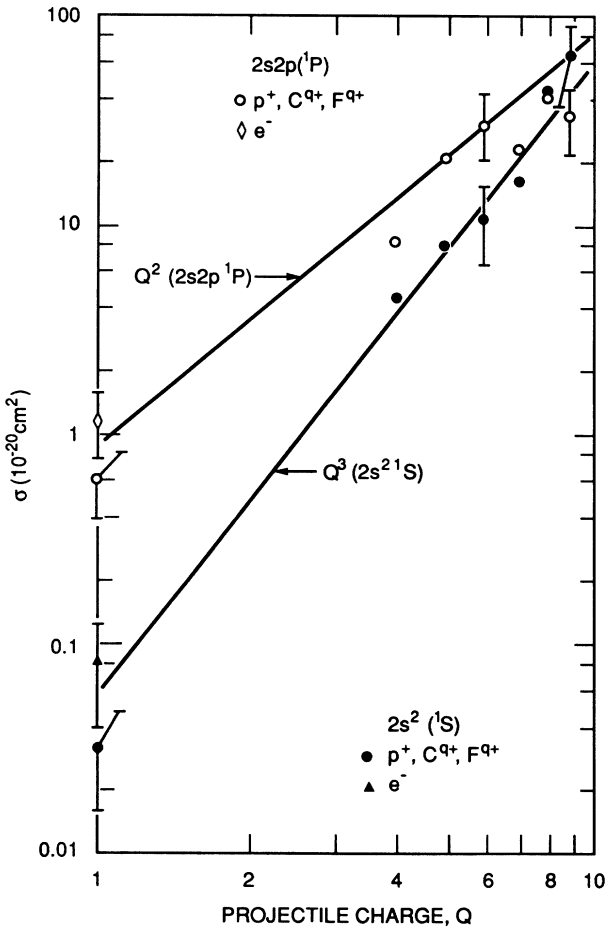

FIG. 8. The total averaged emission cross section from the $2s^2(^1S)$ and $2p^2(^1P)$ states as a function of the projectile charge.

interference between the first- and second-order mechanisms may be unimportant in double excitation by electrons and protons. This conclusion disagrees in part with the calculations of Fritsch and Lin. They find that protons are nearly twice as effective as electrons at exciting the ^1D state and that there is almost no difference between these projectiles for the ^1S and ^1P states.

The charge dependences of the $2s^2(^1S)$ and $2s2p(^1P)$ yields are illustrated in Fig. 8. The solid curves were drawn to guide the eye through a Q^3 dependence for the ^1S and a Q^2 dependence for the ^1P and are not fits. The ^1S state clearly has a much stronger charge dependence. Furthermore, the ^1P yields are fairly constant above $Q=6$, suggesting that the cross section is beginning to saturate. We know from single-excitation measurements[45] that the $1s^2$ to $1s2p$ excitation is saturated for these charges and velocities. If the ^1P state were populated via this excitation followed by a shake, then the ^1P yields might also show signs of saturation. The measured Q^2 dependence supports excitation via the first-order mechanism. The relatively small cross section found for this state could be due to the small shake probability. The total yields for the ^1P state were fit using Eq. (17), giving an exponent B of 1.73 ± 0.35. Arcuni and Schneider observed a similar overall charge dependence with $B=1.55$. They did not see any signs of saturation, but used charges of only $Q=3$ and lower. The theoretical ^1P results shown in Table IV also exhibit no signs of saturation, and increase at a slightly higher rate between Q^2 and Q^3. Note that as discussed above, the theoretical values are considerably larger than the data. Finally, the ^1S state yields were also fit with Eq. (17), giving an exponent of 3.0. This overall dependence is in qualitative agreement with the theory which increases at a rate slightly lower than Q^3. As with the ^1P state, the theoretical results are much larger than the data.

V. CONCLUSIONS

Electron emission yields due to double excitation to the $2s^2(^1S)$, $2p^2(^1D)$, and $2s2p(^1P)$ states of helium have been measured using electron, proton, carbon, and fluorine projectiles at high velocities. The emission yields from these states increase with the projectile charge at rates between Q^2 and Q^3. This is far slower than the Q^4 dependence given by the independent electron model. Hence, our results indicate that electron-electron interactions are important in double-excitation processes. This conclusion is in qualitative agreement with the recent calculations of Fritsch and Lin. Theory and experiment do not agree, however, on the relative magnitude of excitation to the three states we observed. Theory and experiment also disagree on the importance of interference between first- and second-order mechanisms. These differences are probably due to both uncertainties in the present data and to the inherent difficulty in comparing the measured differential emission yields to the calculated double-excitation cross sections. Calculations of the doubly differential electron yields would help resolve this difficulty and might provide more information for interpreting the shapes of the measured spectra. There are also differences between our results and the data of Petersen *et al.*[29] Further experimental work is needed to understand these differences. Improvement of the energy resolution of the spectra so that the ^1D and ^1P could be more clearly resolved would be especially helpful in reducing the uncertainty of the data. Furthermore, measurements over the entire range of emission angles are needed to allow more direct comparisons of experiment and theory.

ACKNOWLEDGMENTS

We thank J. H. McGuire, K. Taulbjerg, and W. Mehlhorn for many helpful discussions. We also thank J. M. Sanders for his advice on the fitting routine. Finally, we thank W. Fritsch and C. D. Lin for use of their calculations prior to publication. This research was sponsored by the U.S. Department of Energy, Office of Basic Energy Sciences, Division of Chemical Sciences, under Contract No. DE-AC05-840R21400 with Martin Marietta Energy Systems, Inc. and by an appointment (J.P.G.) to the U.S. Department of Energy Laboratory Cooperative Postgraduate Research Training Program administered by Oak Ridge Associated Universities.

*Present address: Department of Physics, Kansas State University, Manhattan, KS 66506-2601.

†Present address: LBL Division, Bldg. 2177, L-421, Lawrence Livermore Laboratory, Livermore, CA 94550.

‡Permanent address: Department of Physics, University of North Carolina, Chapel Hill, NC 27514.

§Permanent address: Department of Physics, University of South Alabama, Mobile, AL 36681.

[1]J. H. McGuire, Phys. Rev. A **36**, 1114 (1987).

[2]N. Stolterfoht, Comm. At. Mol. Phys., July (1988).

[3]L. H. Andersen, P. Hvelplund, H. Knudsen, S. P. Moller, K. Elsener, K.-G. Rensfelt, and E. Uggerhoj, Phys. Rev. Lett. **57**, 2147 (1987).

[4]L. H. Andersen, P. Hvelplund, H. Knudsen, S. P. Moller, A. H. Sorensen, K. Elsener, K.-G. Rensfelt, and E. Uggerhoj, Phys. Rev. A **36**, 3613 (1987).

[5]E. Horsdal Pedersen and L. Larsen, J. Phys. B **12**, 4085 (1977).

[6]J. Palinkas, R. Schuch, H. Cederquist, and O. Gustasson, Phys. Rev. Lett. **63**, 2464 (1989).

[7]E. Horsdal, B. Jensen, and K. O. Nielsen, Phys. Rev. Lett. **58**, 1414 (1986).

[8]J. Briggs and K. Taulbjerg, J. Phys. B **12**, 2565 (1979).

[9]T. Ishihara and J. H. McGuire, Phys. Rev. A **38**, 3310 (1988).

[10]H. K. Haugen, L. H. Andersen, P. Hvelplund, and H. Knudsen, Phys. Rev. A **26**, 1962 (1982).

[11]J. F. Reading and A. L. Ford, Phys. Rev. Lett. **58**, 543 (1987).

[12]R. E. Olsen, Phys. Rev. A **36**, 1519 (1987).

[13]L. Vegh, Phys. Rev. A **37**, 992 (1988).

[14]J. H. McGuire, Nucl. Instrum. Meth. Phys. Res. **A262**, 48 (1987).

[15]R. Whiddington and M. Priestly, Proc. R. Soc. London, Ser. A **145**, 462 (1934).

[16]S. M. Silverman and E. N. Lassettre, J. Chem. Phys. **40**, 1265 (1964).
[17]E. Weigold, A. Ugabe, and P. J. O. Teubner, Phys. Rev. Lett. **35**, 209 (1975).
[18]R. P. Madden and K. Codling, Phys. Rev. Lett. **10**, 516 (1963).
[19]W. Melhorn, Phys. Lett. **21**, 155 (1966).
[20]N. Oda, F. Nishimura, and S. Tahira, Phys. Rev. Lett. **24**, 42 (1970).
[21]F. D. Schowengerdt, S. R. Smart, and M. E. Rudd, Phys. Rev. A **7**, 560 (1973), and references therein.
[22]A. Bordenave-Montesquieu, A. Gleizes, and P. Benoit-Cattin, Phys. Rev. A **25**, 245 (1982).
[23]P. van der Straten, R. Morgenstern, and A. Niehaus, J. Phys. B **21**, 1573 (1988).
[24]P. W. Arcuni and D. Schneider, Phys. Rev. A **36**, 3059 (1987), and references therein.
[25]B. Barker and H. W. Barry, Phys. Rev. **151**, 14 (1966).
[26]U. Fano, Phys. Rev. **124**, 1866 (1961).
[27]V. V. Balashov, S. S. Lipovetskii, and V. S. Senashenko, Sov. Phys.—JETP **36**, 858 (1973) [Zh. Eksp. Teor. Fiz. **63**, 1622 (1972)].
[28]A. Bordenave-Montesquieu, P. Benoit-Cattin, M. Rodiere, A. Gleizes, and H. Merchez, J. Phys. B **8**, 874 (1975).
[29]J. O. P. Pedersen and P. Hvelplund, Phys. Rev. Lett. **62**, 2373 (1989). Note: The data of Pedersen and Hvelplund shown here have been corrected to account for more recent measurements by these authors as per their instructions via a private communication.
[30]D. Burch, J. E. Schneider, and C. F. Moore, Phys. Rev. Lett. **36**, 166 (1976).
[31]W. Fritsch and C. D. Lin, Phys. Rev. A **41**, 4776 (1990).
[32]J. K. Swenson, J. M. Anthony, M. Reed, M. Benhenni, and S. M. Shafroth, Nucl. Instrum. Methods Phys. Res. **B24/25**, 184 (1987).
[33]C. W. Woods, R. L. Kauffman, K. A. Jamison, N. Stolterfoht, and P. Richard, Phys. Rev. A **13**, 1358 (1976).
[34]J. L. Wiza, Nucl. Instrum. Methods Phys. Res. **162**, 587 (1979).
[35]M. E. Rudd, L. H. Toburen, and N. Stolterfoht, Atm. Data Nucl. Data Tables **18**, 413 (1976).
[36]H. Platten, G. Schiwietz, T. Schneider, D. Schneider, W. Zeitz, K. Musiol, T. Zouros, R. Kowallik, and N. Stolterfoht, *Book of Contributed Abstracts, Proceedings of the 15th International Conference on the Physics of Electronic and Atomic Collision,* Brighton, 1987 (North-Holland, Amsterdam, 1987), p. 437.
[37]P. D. Fainstein, V. H. Ponce, and R. D. Rivarola, J. Phys. B **21**, 287 (1988).
[38]B. W. Shore, Rev. Mod. Phys. **39**, 439 (1967).
[39]S. S. Lipovetsky and V. S. Senashenko, J. Phys. B **7**, 693 (1974).
[40]S. Bashkin and J. O. Stoner, *Atomic Energy Levels & Grotian Diagrams* (North-Holland, Amsterdam, 1975), Vol. 1, p. 11.
[41]W. Shearer-Izumi, Atm. Data Nucl. Data Tables **20**, 531 (1977).
[42]P. van der Straten and R. Morgenstern, J. Phys. B **19**, 1361 (1986).
[43]P. W. Arcuni, Phys. Rev. A **33**, 105 (1986).
[44]A. Gleizes, P. Benoit-Cattin, A. Bordenave-Montesquieu, and H. Merchez, J. Phys. B **9**, 473 (1976).
[45]K. Reymann, K.-H. Schartner, and B. Sommer, Nucl. Instrum. Meth. Phys. Res. **B23**, 157 (1987).
[46]J. H. McGuire, A. Muller, B. Schuch, W. Groh, and E. Salzborn, Phys. Rev. A **35**, 2479 (1987).
[47]J. H. McGuire, A. Muller, B. Schuch, W. Groh, and E. Salzborn, Phys. Rev. A **35**, 2479 (1987).